Boundary-Layer Meteorol (2010) 136:285–299
DOI 10.1007/s10546-010-9508-x

ARTICLE

Synthetic-Eddy Method for Urban Atmospheric Flow Modelling

D. Pavlidis · G. J. Gorman · J. L. M. A. Gomes · C. C. Pain · H. ApSimon

Received: 13 April 2009 / Accepted: 12 May 2010 / Published online: 28 May 2010

Abstract The computational fluid dynamics code Fluidity, with anisotropic mesh adaptivity, is used as a multi-scale obstacle-accommodating meteorological model. A novel method for generating realistic inlet boundary conditions based on the view of turbulence as a superposition of synthetic eddies is adopted. It is able to reproduce prescribed first-order and second-order one-point statistics and turbulence length scales. The aim is to simulate an urban boundary layer. The model is validated against two standard benchmark tests: a plane channel flow numerical simulation and a flow past a cube physical simulation. The performed large-eddy simulations are in good agreement with both reference models giving confidence that the model can be used to successfully simulate urban atmospheric flows.

Keywords Adaptive mesh · Inlet boundary conditions · Large-eddy simulation

1 Introduction

In a limited-area numerical flow simulation, the inlet boundary conditions account for any influence upwind of the area of interest that is not included in the computational domain. To a large extent, they determine the solution inside the computational domain (Franke et al. 2007). Therefore, their treatment and prescription need to be carefully considered before they are applied.

In Reynolds-averaged Navier–Stokes (RANS) methods the mean velocity profile and information about the turbulence quantities kinetic energy (k) and energy dissipation rate (ε) are required for a $k-\varepsilon$ model (Franke et al. 2007). In large-eddy simulation (LES) and direct numerical simulation methods the procedure of generating realistic inlet boundary conditions is somewhat more complicated since time dependent boundary conditions are required.

D. Pavlidis (✉) · G. J. Gorman · J. L. M. A. Gomes · C. C. Pain
Department of Earth Science and Engineering, Imperial College London, London SW7 2AZ, UK
e-mail: dimitrios.pavlidis@imperial.ac.uk

H. ApSimon
Centre for Environmental Policy, Imperial College London, London SW7 2AZ, UK

A number of techniques have been successfully applied for a wide range of applications, and the most fundamental ones are briefly reviewed here.

Kondo et al. (1997) used the method of Hoshiya (1972) based on Monte Carlo simulation considering power spectral density and cross-spectral density as targets. Lund (1998) divided the computational domain in two parts: one near the inlet plane being periodic and one following the stream-wise direction. In each recirculation of the field he used a modified version of rescaling the field of the original method proposed by Spalart and Leonard (1985). Another approach is the use of precursor simulations, from which data are extracted to form inlet boundary conditions for the main simulation (Thomas and Williams 1999). Smirnov et al. (2001), based on earlier methods for synthesising divergence-free vector fields from a sample of Fourier harmonics (Kraichnan 1970), generated non-homogeneous, anisotropic flow fields representing turbulent velocity fluctuations. Klein et al. (2003) used a digital filter approach to simulate a non-homogeneous, anisotropic turbulent field. A random three-dimensional flow field is filtered using a filter operation and a coordinate transformation using Lund's method, resulting in two-dimensional arrays of spatially correlated data. It essentially represents an alternative approach to Lee et al. (1992) who used an inverse Fourier transform on a discrete signal to model turbulence. Xu and Martin (2004) extended the method of Lund (1998) by using a different rescaling method based on Morkovin's hypothesis and generalised temperature–velocity relationships. Druault et al. (2004) used proper orthogonal decomposition and linear stochastic estimation to generate realistic inlet conditions. Kempf et al. (2005) using a diffusion process and Lund (1998)'s decomposition converted white noise into a signal that features the required length scale and Reynolds stresses. This method was designed to be used in arbitrary geometries. Majander (2006) used Kempf et al.'s method to simulate flow through a channel, while di Mare et al. (2006) extended the work of Klein et al. (2003) using a more detailed method of calculating the filter coefficients. They concluded that the simple approach suffices for free flows, while the more detailed approach provides much better results in wall-bounded flows. Jarrin et al. (2006) produced realistic inflow conditions using a method based on the classical view of turbulence as a superposition of coherent structures. This method is able to reproduce prescribed first-order and second-order one-point statistics, characteristic length and time scales, and the shape of coherent structures. In Jarrin et al. (2009) the same method is applied on a hybrid LES/RANS model. Finally, Xie and Castro (2008) used a digital-filter based technique taking into account that correlation functions of turbulent flows have forms not to dissimilar to decaying exponentials.

In most urban atmosphere and street canyon studies either periodic boundary conditions or a long computational domain before the area of interest are used in order to obtain a realistic representation of the lower atmospheric boundary layer. Roughness elements have also been added in some studies before the area of interest in order to imitate the wind-tunnel technique for generating turbulence. Periodic boundaries recycle the wind field in the streamwise and span-wise directions until the desired field is developed. Nozawa and Tamura (2002) used the method of Lund (1998) (modified periodic) along with roughness elements on the bottom. Very long computational domains in the streamwise direction have also been used so that turbulence evolves naturally (Nakayama et al. 2005).

In this study, Fluidity,[1] a general purpose computational fluid dynamics (CFD) code, with anisotropic mesh adaptivity (Pain et al. 2001), is used as a multi-scale obstacle-accommodating meteorological model. Past studies using the Fluidity code to simulate air flows and pollutant dispersion in the urban atmospheric environment (Bentham 2003; Wang 2007) have concluded, that even though the model performed well, it was unable to generate a

[1] http://amcg.ese.ic.ac.uk/Fluidity.

fully developed deep turbulent boundary layer. This shortcoming was considered to have originated from the lack of inlet boundary conditions treatment.

The synthetic-eddy method for generating realistic inlet boundary conditions developed by Jarrin et al. (2006) is adopted here to model the urban boundary layer. The method is based on the view of turbulence as a superposition of coherent structures, and is computationally inexpensive, designed for use with unstructured meshes, and the generated condition satisfies the prescribed mean velocities, Reynolds stress tensor and turbulence length scales. In practice, Doppler sonic detection and ranging (SODAR) and light detection and ranging (LIDAR) data (Barlow 2008) can be used as input for this method. This can increase the accuracy of the prescribed statistics that are usually crudely estimated, or taken from reference physical or numerical simulations.

The objectives of our study are to improve the performance and the confidence in the results of Fluidity for atmospheric flow modelling. The recommendations from COST Action 732 (Britter and Schatzmann 2007) are followed for model set-up purposes and the model evaluation strategy. COST Actions are networks centred around European nationally funded research projects. COST Action 732 was developed to improve and assure the quality of micro-scale meteorological models that are applied for predicting flow and transport processes in urban, or industrial environments.

The remainder of this paper is organised as follows. The fluid model along with the synthetic-eddy method are described in Sect. 2. The test cases considered are presented in Sect. 3. Finally, some concluding remarks are given in Sect. 4.

2 Fluid Model

2.1 Governing Equations

In LES the larger scales of motions are numerically resolved while the effect of the smaller scales is modelled. This is accomplished by filtering the velocity field (U) according to:

$$\overline{U}(x,t) = \int_D G(r,x)\, U(x-r,t) dr, \tag{1}$$

where the overbar denotes a filtered quantity, D is the computational domain, x represents the Cartesian coordinates, r represents the radial coordinates, G represents the filter function and t is time. The filter has the effect of removing those scales of motion smaller than the filter width F. The specified filter function G satisfies the normalisation condition:

$$\int_D G(r,x)\, dr = 1. \tag{2}$$

The residual field is defined by:

$$u'(x,t) \equiv U(x,t) - \overline{U}(x,t). \tag{3}$$

The incompressible Navier–Stokes equations of the filtered quantities, provided that the filter remains invariant in space and time, can be written as the continuity equation:

$$\frac{\partial \overline{U}_i}{\partial x_i} = 0 \tag{4}$$

and the momentum equation:

$$\frac{\partial \overline{U}_i}{\partial t} + \overline{U}_j \frac{\partial \overline{U}_i}{\partial x_j} = -\frac{1}{\rho}\frac{\partial \overline{p}}{\partial x_j} + \frac{\partial}{\partial x_j}\left[\nu\left(\frac{\partial \overline{U}_i}{\partial x_j} + \frac{\partial \overline{U}_j}{\partial x_i}\right) + \tau_{ij}\right], \tag{5}$$

where ρ is the density, p is the pressure and ν is the kinematic viscosity. The effect of the unresolved scales is added in the momentum equation through the stress term τ_{ij}, called the subgrid-scale (SGS) tensor, and given by:

$$\tau_{ij} = \overline{U}_i \overline{U}_j - \overline{U_i U_j}. \tag{6}$$

The second term in the SGS tensor cannot be calculated directly using information from the resolved field.

Assuming that the unresolved scales act primarily to drain energy from the resolved scales, in the same way that molecular viscosity removes energy from a laminar flow, the filtered momentum equation (Eq. 5) can be written as:

$$\frac{\partial \overline{U}_i}{\partial t} + \overline{U}_j \frac{\partial \overline{U}_i}{\partial x_j} = -\frac{1}{\rho}\frac{\partial \overline{P}}{\partial x_j} + \frac{\partial}{\partial x_j}\left[(\nu + \nu_\tau)\left(\frac{\partial \overline{U}_i}{\partial x_j} + \frac{\partial \overline{U}_j}{\partial x_i}\right)\right], \tag{7}$$

where $\overline{P}$ is a modified pressure term and ν_τ is the SGS viscosity. The model used to calculate the SGS viscosity is a variation of the Smagorinsky model (Smagorinsky 1963) originally developed by Bentham (2003). The advantage of the SGS model used here, over the original Smagorinsky model, is that the length scale is related directly to the local length scale of the flow, and is allowed to vary in space and direction, rather than being fixed and predetermined. Fourth-order dissipation is achieved by subtracting out two discretisations of the same second-order operator (Candy 2008). This fourth-order discretisation is used to compensate for the dissipation issues associated with the original Smagorinsky model and the use of tetrahedral meshes. More details on the SGS model can be found in Bentham (2003) and Candy (2008).

The Navier–Stokes equations are discretised in space and time using the Bubnov–Galerkin and Crank–Nicholson methods, respectively. More details on the numerical method used by Fluidity and the adaptive mesh algorithm can be found in Mansoorzadeh et al. (1998) and Pain et al. (2001), respectively.

Adaptive, unstructured meshes are used throughout this study. Unstructured meshes have been criticised for not being accurate in LES, and in order to achieve similar results to structured meshes the computational cost of using unstructured meshes is higher. It has been found that by using adaptive meshes, and thus resolving the flow where needed, discrepancies become negligible, while computational cost is kept low (Pain et al. 2001). The results presented here support this theory. A sensitivity analysis on the resolution required by Fluidity to reproduce realistic flows when using adaptive, unstructured meshes can be found in Garcia et al. (2010).

2.2 Synthetic-Eddy Method

The method employed for generating inlet boundary conditions was developed by Jarrin et al. (2006), and is based upon the view of turbulence as coherent structures. The velocity field on the inlet boundary plane is decomposed to a mean and a fluctuating component:

$$U_{in}(x,t) \equiv \overline{U}_{in}(x) + u'_{in}(x,t). \tag{8}$$

In order to calculate the boundary condition for the velocity field, the mean and fluctuating components have to be computed. Assuming steady state, the mean component $\overline{U}_{in}(x)$ is

time invariant, and it is a function of space and usually only the streamwise direction is given a value. The fluctuating component $u'_{in}(x,t)$ is time varying.

In order to calculate the fluctuating component, a number of coherent structures (turbulent spots) are introduced around the inlet plane of the computational domain and are defined by a shape function that encompasses the structures' spatial and temporal characteristics. These structures are generated within a bounding box surrounding the inlet plane to ensure that the latter is statistically covered by them. For a rectangular plane aligned with the Cartesian coordinate system, the dimensions of the bounding box are: $[-l_i(x)^{max} - x_i^{min,s}, +l_i(x)^{max} + x_i^{max,s}] \times [-l_j(x)^{max} - x_j^{min,s}, +l_j(x)^{max} + x_j^{max,s}] \times [-l_k(x)^{max} - x_k^{min,s}, +l_k(x)^{max} + x_k^{max,s}]$, where $l_i(x)^{max}$ is the maximum length scale of the induced turbulence and $x_i^{min,s}$ and $x_i^{max,s}$ are the minimum and maximum of the coordinates of the surface mesh (superscript s) for each direction (i, j, k). The shape function of the turbulent spot, $f_\sigma(x)$, has compact support on the interval $[-l_i(x), +l_i(x)]$ and satisfies the normalisation condition:

$$\frac{1}{\Delta}\int_{-\Delta/2}^{\Delta/2} f_\sigma^2(x)dx = 1, \tag{9}$$

where $\Delta = x^s_{i,max} - x^s_{i,min} + 2l_i(x)$.

The eddies are advected through the bounding box with the bulk velocity of the inlet surface (U_b) using Taylor's frozen turbulence hypothesis: $x_\sigma(t+dt) = x_\sigma(t) + U_b dt$, where x_σ is the location of spot σ and dt the model timestep. Once the spot reaches the downwind surface of the bounding box, it is regenerated at a new location on the upwind surface of the bounding box. The fluctuating component of the velocity field at a node on the inlet plane is given by:

$$u'_{in,\,i}(x,t) = \frac{1}{\sqrt{N}}\sum_{\sigma=1}^{N} \varepsilon_{\sigma,\,i} f_i(x - x_\sigma(t)), \tag{10}$$

where $\varepsilon_{\sigma,\,i}$ is the sign of the spot σ on the component i and is randomly drawn to be $+1$, or -1 and N is the prescribed number of turbulent spots. When regenerating a spot, $\varepsilon_{\sigma,\,i}$ is re-evaluated. The number of turbulent spots N should be large enough to ensure Gaussian behaviour of the fluctuating component in each direction. In real urban environments this is hardly ever the case and this approach is adopted for simplicity. However, in practice it performs well. In this study N is set to 4,000.

It can be shown (Jarrin et al. 2006) that the resulting fluctuating component field is of zero mean, unit variance and that the two-point autocorrelation function reads:

$$R_{uu}(r) = \frac{1}{\Delta}\int_{-\Delta/2}^{\Delta/2} f_\sigma(x) f_\sigma(x+r)dx. \tag{11}$$

and so inflow data with any autocorrelation function can be created. However, the process of determining $f_\sigma(x)$ from Eq. 11 is complex and therefore $f_\sigma(x)$ is chosen a priori.

In Jarrin et al. (2006) the Gaussian function was used to describe the eddies, although in Jarrin et al. (2009) and Jarrin (2003) the triangular function (Eq. 12) was adopted. In this study the latter is used as well.

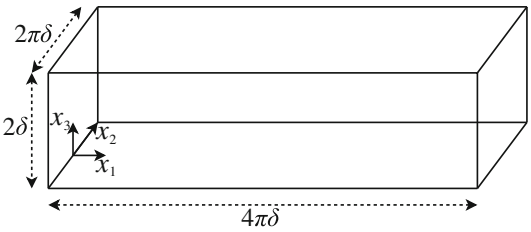

Fig. 1 Schematic of the computational domain for the plane channel flow simulation

$$f(x) = \begin{cases} \sqrt{\frac{3}{2}}(1 - |x|), & \text{if } x < l \\ 0, & \text{otherwise.} \end{cases} \tag{12}$$

The final boundary condition is reconstructed according to Lund (1998): $U_{in,\,i} = \overline{U}_{in,\,i} + \alpha_{ij} u'_{in,\,j}$, where α_{ij} is the amplitude tensor and is related to the Reynolds stress tensor (R_{ij}) through:

$$\alpha_{ij} = \begin{pmatrix} \sqrt{R_{11}} & 0 & 0 \\ R_{21}/\alpha_{11} & \sqrt{R_{22} - \alpha_{21}^2} & 0 \\ R_{31}/\alpha_{11} & (R_{32} - \alpha_{21}\alpha_{31})/\alpha_{22} & \sqrt{R_{33} - \alpha_{31}^2 - \alpha_{32}^2} \end{pmatrix}. \tag{13}$$

3 Results

3.1 Plane Channel Flow

Direct numerical simulation C.32: Channel Flow (Kim et al. 1987) from the ERCOFTAC '*Classic Collection*' Database[2] is reproduced using Fluidity. The Reynolds number (based on the channel half depth, δ, and the centre-line velocity) is 3,300, while the friction Reynolds number (based on δ and the friction velocity u_*) is 180. The dimensions of the computational domain are $4\pi\delta \times 2\pi\delta \times 2\delta$ (in the x_1, x_2 and x_3 directions, respectively). A schematic of the computational domain is given in Fig. 1.

An adaptive tetrahedral mesh with a maximum of 1,500,000 nodes is used. The element edge length in the near-wall region is constrained to $3x_3^+$ in all the wall-normal direction, while in the middle of the domain it is $20x_3^+$, where x_3^+ is the distance from the wall in wall units, defined as $x_3^+ = x_3 u_*/\nu$. The transition from the finer regions to the coarser ones is smooth with the use of a linear gradation parameter of 1.3 in the mesh adaptivity algorithm (i.e. the adjacent element edge length difference does not exceed 30%). However, this constraint is never reached and neighbouring elements have similar edge lengths. The mesh is adapted every ten timesteps. The adaptation is driven by the interpolation error relative to the velocity field, and is set to 0.1, indicating a 10% relative error tolerance for the velocity field (see Pain et al. 2001).

No-slip Dirichlet boundary conditions ($U = 0$) are applied strongly on the solid walls (top and bottom) and free-slip boundary conditions are applied on the lateral sides of the domain. The outflow plane is treated as an open boundary. The synthetic-eddy method is applied on the inlet plane. Periodic boundary conditions are not used because of the use of an adaptive

[2] http://cfd.mace.manchester.ac.uk/ercoftac/index.html.

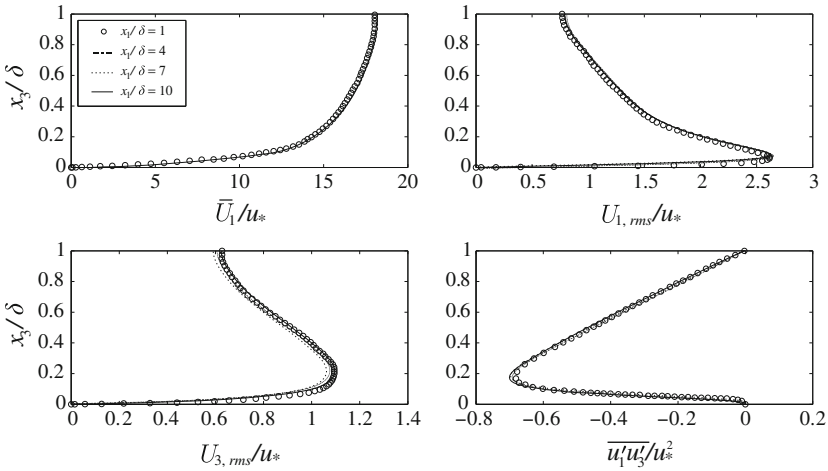

Fig. 2 Convergence to a fully-developed boundary-layer flow of the plane channel test case for the lower half of the computational domain

mesh, which does not ensure that inflow and outflow plane surface meshes are going to be the same, incorporating additional interpolation errors.

Quantities used to generate the inflow conditions include mean velocities, diagonals of the Reynolds stress tensor and the turbulence length scale. Mean velocities and Reynolds stress tensor diagonal components are taken from Kim et al. (1987). Cross-products are not prescribed because not all of them are known, and the turbulence length scale is approximated as in Xie and Castro (2008).

An adaptive timestep is used to satisfy a Courant–Friedrich–Lewy (CFL) number equal to unity. The averaging period for the data presented is 30 non-dimensional time units (δ/u_*) after steady state has been reached ($\approx$20 non-dimensional time units). Since the timestep is not constant, linear interpolation is employed to evenly distribute time for post-processing.

The convergence of the development of the flow parameters is given in Fig. 2, where vertical profiles include 65 sampling points. Profiles are averaged spatially over the lateral extent of the domain, with 20 equidistant profiles used for this averaging process. The mean streamwise velocity $\overline{U}_1/u_*$, the root-mean-square velocities $U_{i,\,rms}/u_*$ (defined as $(\overline{u_i'u_i'})^{1/2}/u_*$) and the Reynolds shear stress (defined as $\overline{u_1'u_3'}/u_*^2$) practically remain unchanged. It is evident that, even though the Reynolds shear stress is not prescribed (assumed zero) at the inflow plane, it recovers its true value very quickly. An instantaneous cut for a plane parallel to one lateral boundary ($x_2/\delta = -0.95\pi\delta$) and the inflow plane ($x_1/\delta = 0$) of the mesh and the total lateral velocity component (U_2/u_*) at time $t = 20$ is shown in Fig. 3.

Comparison of flow mean and turbulent quantities between the two models is given in Fig. 4. Spatial convergence profiles are averaged to compute these profiles. Results are in good agreement to the reference data. Numerical experiments (not presented here) show that large grid size changes in the near-wall region in the vertical direction result in turbulent quantities' peak shift and an exaggerated laminar sub-layer near the solid wall. When using gradually finer meshes the profiles converge to the reference data and the laminar sub-layer shrinks. The fine mesh used therefore is essential for obtaining good agreement with the reference data. The reason for this is the absence of wall boundary conditions.

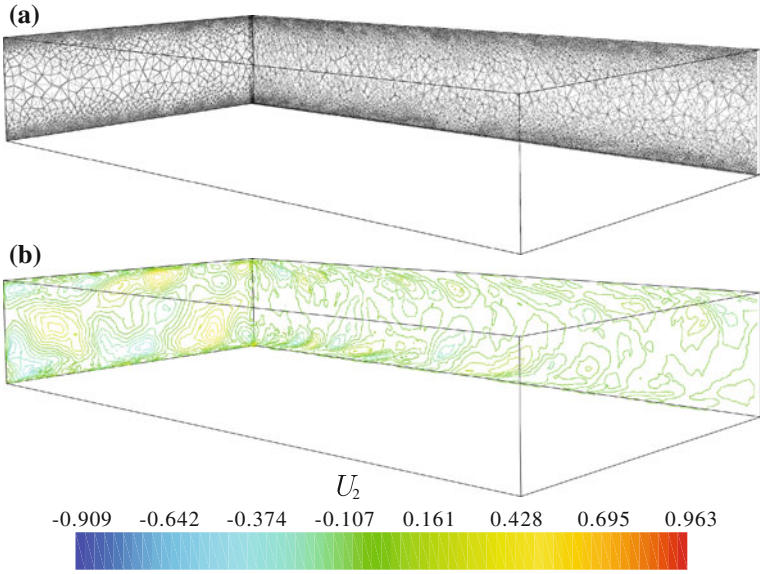

Fig. 3 Instantaneous mesh (**a**) and instantaneous total lateral velocity (U_2/u_*) contours (**b**) for a plane parallel to one lateral boundary ($x_2/\delta = -0.95\pi\delta$) and the inflow ($x_1/\delta = 0$) plane at time $t = 20$

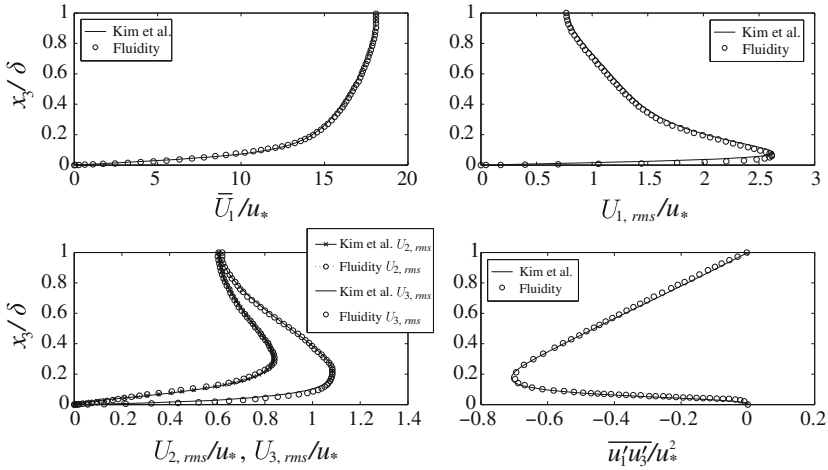

Fig. 4 Comparison of mean velocity, r.m.s. velocity and Reynolds shear stress between Kim et al. (1987) and Fluidity for the lower half of the domain. Spatial convergence profiles are averaged to compute these profiles

3.2 Flow Past a Bluff Body

In order to evaluate the capability of Fluidity simulating accurately atmospheric flows under and over roof-top level the classical test case of flow past a bluff body is chosen. For this simulation the test case A1-4 from the 'CEDVAL' database[3] is used as reference.

[3] http://www.mi.uni-hamburg.de/Introduction.433.0.html.

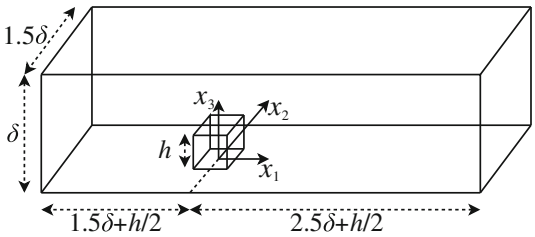

Fig. 5 Schematic of the computational domain for the flow past the bluff body simulation

The Reynolds number (based on the boundary-layer depth δ and the maximum velocity) is 37,250, while the friction Reynolds number (based on δ and the friction velocity u_*) is 7,450. The dimensions of the computational domain are identical to those of the wind tunnel apart from the development area, which is placed 1.5δ upwind of the bluff body. The cross-sectional area is $1.5\delta \times \delta$, in the lateral and vertical directions, respectively. The side (h) of the bluff body is $0.125/\delta$ and the centre of the body itself is placed at $(0, 0, 0.125/2\delta)$ in the x_1, x_2 and x_3 directions, respectively. A schematic of the computational domain in shown in Fig. 5.

An adaptive tetrahedral mesh with a maximum of 550,000 nodes is used. The element edge length in the near-wall region of all solid walls (i.e. bluff body, sides, top, bottom) is constrained to $h/20$. This is also true for a $2.5h$ distance around the bluff body in all three directions. In the upper part of the domain the element edge length is $\delta/20$. The transition from the finer regions of the mesh to the coarser ones is smooth with the use of a linear gradation parameter of 1.3 in the mesh adaptivity algorithm (i.e. adjacent element edge length difference does not exceed 30%). However, this constraint is never reached and neighbouring elements have similar edge lengths. The mesh is adapted every ten timesteps. The adaptation is driven by the interpolation error relative to the velocity field. This is set to 0.15, indicating a 15% relative error tolerance for the velocity field (see Pain et al. 2001). No-slip Dirichlet boundary conditions ($U = 0$) are applied strongly on all solid walls, while the outflow plane is treated as an open boundary. The synthetic-eddy method is applied on the inlet plane.

Quantities used to generate the inflow conditions include mean velocities, diagonals of the Reynolds stress tensor and turbulence length scale. Mean velocities and Reynolds stress tensor diagonal components are taken from the wind tunnel approaching flow data.[4] Cross-products are not prescribed because not all of them are known. The turbulence length scale is empirically set to $\delta/5$ for all three directions and over the whole inflow plane (i.e. isotropic and constant).

An adaptive timestep is used to satisfy a CFL number equal to 1.5. The averaging period for the data presented is 30 non-dimensional time units (δ/u_*) after steady state is reached, with steady state considered to have been reached after first-order and second-order flow statistics remain unchanged and roughly unchanged, respectively, over periods of 5 through-flows. A through-flow is defined as the time needed for the flow to cross the domain ($T_\delta = (h + 4\delta)/U_b$), where U_b is the inflow plane bulk velocity. A through-flow is considerably larger than the large-eddy turnover time defined as: $T_\lambda = \lambda/U_\lambda$, where λ is the large-eddy length scale and velocity, respectively (see van Veen et al. 2006; Oliveira et al. 2007). Since the timestep is not constant, linear interpolation is employed to evenly distribute time for post-processing.

Diagnostics for this simulation include the mean streamwise ($\overline{U}_1/u_*$) and vertical ($\overline{U}_3/u_*$) components of the velocity field and the Reynolds shear stress ($\overline{u'_1 u'_3}/u_*^2$). The friction velocity

[4] http://www.mi.uni-hamburg.de/A1-4.632.0.html.

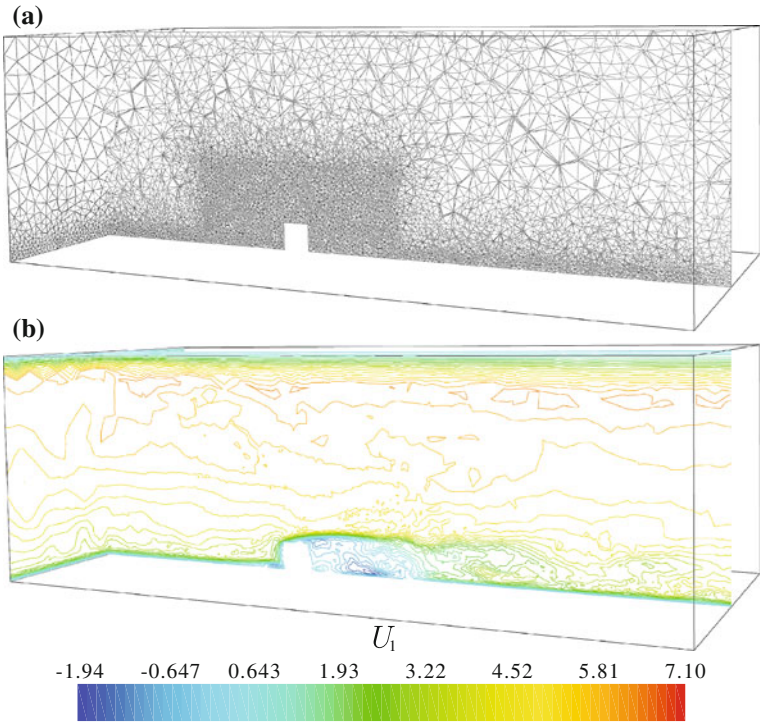

Fig. 6 Instantaneous mesh (**a**) and instantaneous total streamwise velocity (U_1/u_*) contours (**b**) for the vertical symmetry ($x_2/\delta = 0$) and inflow ($x_1/\delta = -1.5\delta - h/2$) planes at time $t = 20$

(u_*) is determined through the friction Reynolds number definition and is used for non-dimensionalisation purposes. Root-mean-square quantities of velocity have been omitted to avoid the inclusion of a large number of plates. No spatial averaging is undertaken in this analysis. All profiles are taken at the vertical symmetry plane ($x_2/\delta = 0$). An instantaneous cut for the vertical symmetry ($x_2/\delta = 0$) and the inflow ($x_1/\delta = -1.5\delta - h/2$) planes of the mesh and the total streamwise velocity component (U_1/u_*) at time $t = 20$ are shown in Fig. 6.

Comparisons for the flow mean and turbulent quantities between the two models are given in Figs. 7, 8 and 9. The results are comparable even though some discrepancies are evident. The Reynolds shear stress is significantly under-predicted at $x_1/\delta = -0.3125$ (see Fig. 9), but gradually evolves to its true value just before the bluff body. This is considered to have originated from the very poor estimation of the turbulence length scale. Nevertheless, the results are encouraging since, even though the turbulence length scale is not accurately prescribed, the flow is able to fully develop within a short distance. As far as the flow around the body is concerned, the flow separation over the top of the body is in good agreement with the reference data. However, the flow in the wake of the body reattaches slightly earlier than the reference data, which is a common characteristic of Smagorinsky-type LES models.

Figure 10 shows the power spectrum $E(f)$ of turbulence produced by Fluidity, where the sampling point is placed in the wake of the bluff at a height $1.5h$. The lower-frequency end ($f < 50$) of this spectrum has a reasonable shape, being flat, while at medium frequencies ($f \approx 50$–150) the power spectrum decreases with a gradient of about $-5/3$. This is the same as the gradient of the Eulerian time spectrum predicted by turbulence theory in the inertial subrange of turbulence. At higher frequencies ($f > 150$) the power spectrum stabilises.

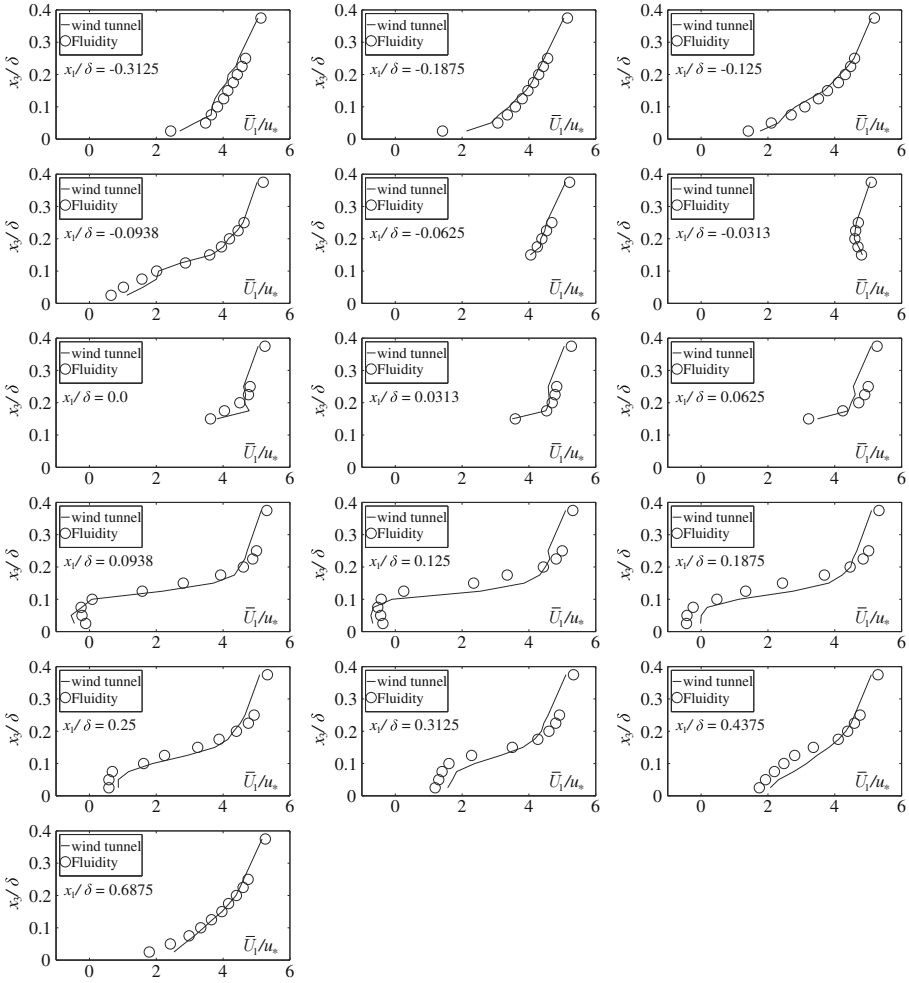

Fig. 7 $\overline{U}_1/u_*$ profiles at the vertical symmetry plane ($x_2/\delta = 0$)

4 Conclusions

A novel method for simulating atmospheric flows using a mesh-adaptive LES in combination with the synthetic-eddy method has been presented. The resulting model was assessed for its ability to generate features of the atmospheric boundary layer. It was able to reproduce first-order and second-order one-point statistics, turbulence length and time scales, and was evaluated using two benchmark test cases: the plane channel flow numerical simulation of Kim et al. (1987) and the flow past a bluff body physical simulation of the 'CEDVAL' database.

For the first test case, with the exception of Reynolds stress tensor cross-products (assumed zero), inflow statistics were accurately prescribed. The absence of wall boundary conditions rendered the model highly mesh dependent. Nevertheless, the use of gradually tighter tolerances for the adaptation of the mesh resolved the near-wall region and the solution converged

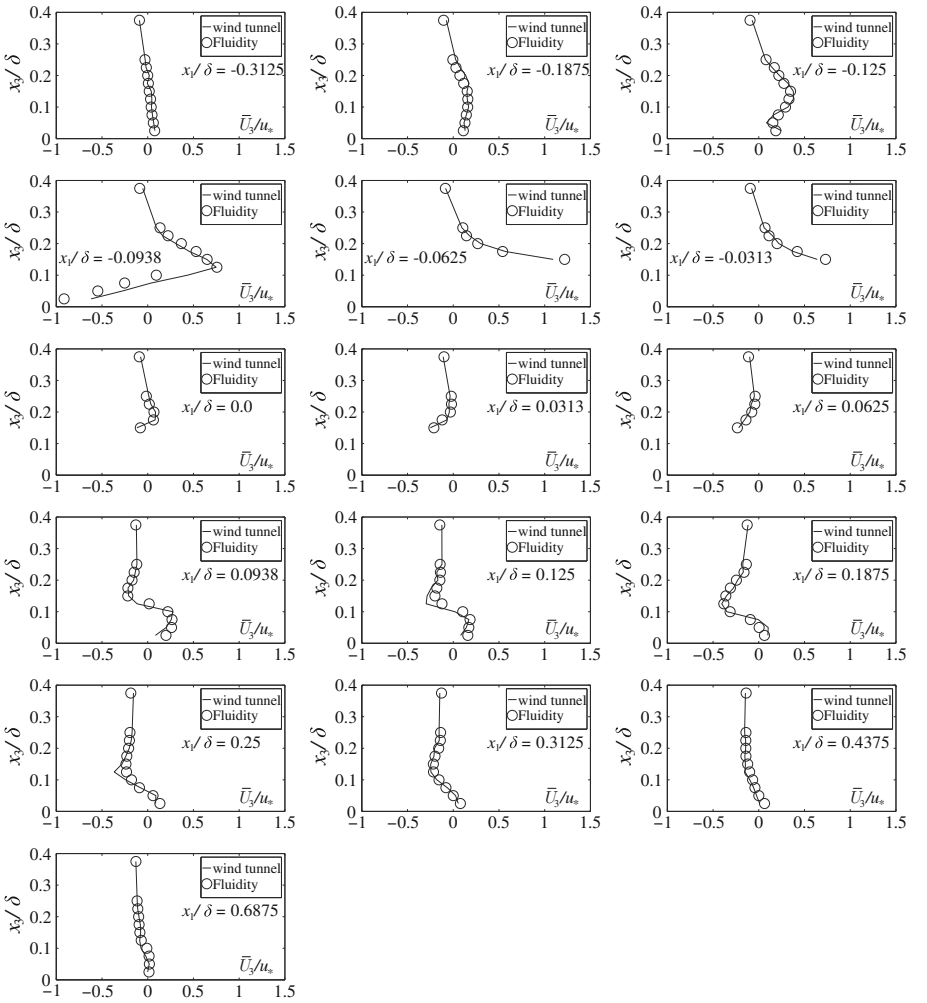

Fig. 8 $\overline{U}_3/u_*$ profiles at the vertical symmetry plane ($x_2/\delta = 0$)

to the reference. It was also concluded that the Reynolds shear stress recovered its true value rapidly giving nominal spatial variations at different planes downwind and indicating that the method is insensitive to the prescription of second-order cross-products.

For the second test case, inflow statistics were more crudely prescribed. The Reynolds stress tensor cross-products were again assumed zero and the turbulence length scale was only empirically calculated. Nevertheless, the model was able to recover second-order statistics within two boundary-layer depths and the results matched reference data downwind of that inflow development area. The mesh used in this test case was significantly coarser than the one in the previous one indicating that in form drag dominated problems the model is not mesh dependent.

Taken together, the results presented here established with sufficient confidence that the model can be used to successfully and efficiently simulate flow in urban areas. The development area upwind of the area of interest has been drastically reduced and the approach

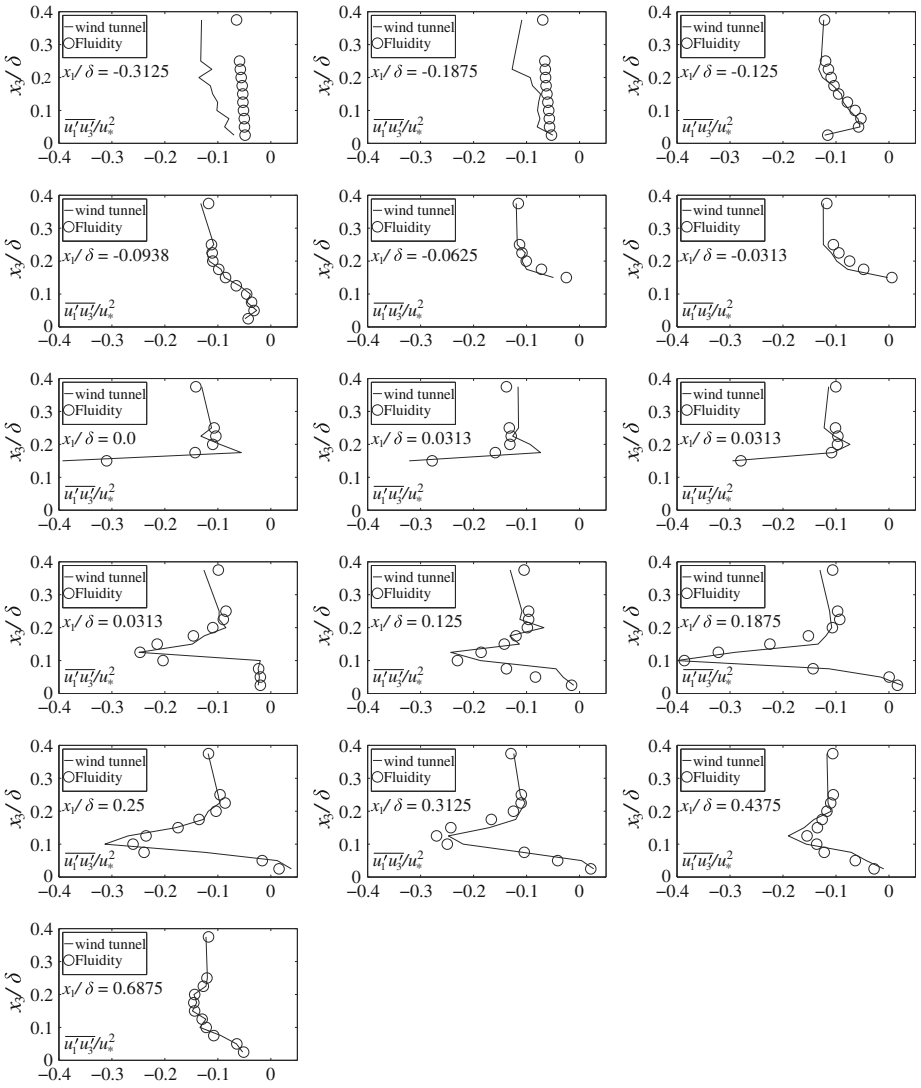

Fig. 9 Reynolds shear stress ($\overline{u_1'u_3'}/u_*^2$) profiles at the vertical symmetry plane ($x_2/\delta = 0$)

flow satisfies prescribed statistics. Even in the case of poorly prescribed quantities the flow is able to fully develop in an area of about two boundary-layer depths. Future work includes coupling this method to a mesoscale meteorological model such as MM5[5] and comparing the simulations against Doppler SODAR and LIDAR urban atmospheric data (see Barlow 2008).

[5] http://www.mmm.ucar.edu/mm5/.

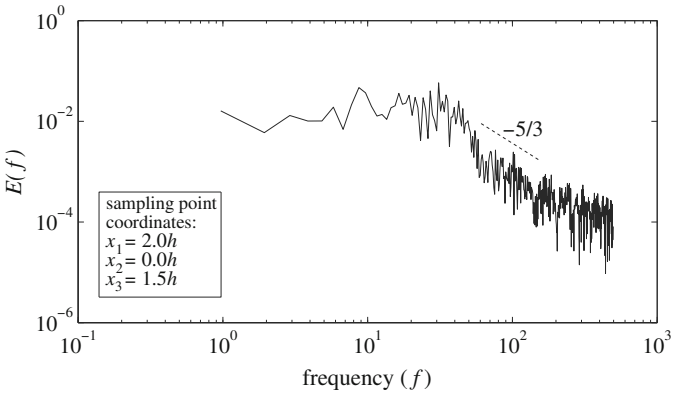

Fig. 10 Power spectrum E produced from Fluidity at a point in the cube wake. The *dashed line* has a gradient of $-5/3$

References

Barlow JF (2008) Using remote sensing to measure wind and turbulence profiles over UK cities. In: 8th wind engineering society UK conference on wind engineering (WES-08), Surrey, UK, 14–16 July, 4 pp

Bentham JHT (2003) Microscale modelling of air flow and pollutant dispersion in the urban environment. PhD thesis, Imperial College London, 271 pp

Britter R, Schatzmann M (2007) Background and justification document to support the model evaluation guidance and protocol, COST Action 732. COST Office Brussels, 88 pp

Candy AS (2008) Subgrid scale modelling of transport processes. PhD thesis, Imperial College London, 356 pp

di Mare L, Klein M, Jones WP, Janicka J (2006) Synthetic turbulence inflow conditions for large-eddy simulation. Phys Fluids 18(025107), 11 pp

Druault P, Lardeau S, Bonnet JP, Coiffet F, Delville J, Lamballais E, Largeau JF, Perret L (2004) Generation of three-dimensional turbulent inlet conditions for large-eddy simulation. AIAA J 42(3):447–456

Franke J, Hellsten A, Schluenzen H, Carissimo B (2007) Best practice guideline for the CFD simulation of flows in the urban environment, COST Action 732. COST Office, 52 pp

Garcia X, Pavlidis D, Gorman GJ, Gomes JLMA, Piggott MD, Aristodemou E, Mindel J, Latham J-P, Pain CC, ApSimon H (2010) A two-phase adaptive finite element method for solid-fluid coupling in complex geometries. Int J Numer Methods Fluids. doi:10.1002/fld.2249

Hoshiya M (1972) Simulation of multi-correlated random processes and application to structural vibration problems. In: Proceedings of JSCE, vol 204, 7th edn, pp 121–128

Jarrin N (2003) Synthetic inflow boundary conditions for the numerical simulation of turbulence. PhD thesis, University of Manchester, 258 pp

Jarrin N, Benhamadouche S, Laurence D, Prosser R (2006) A synthetic-eddy-method for generating inflow conditions for large-eddy simulations. Int J Heat Fluid Flows 27:585–593

Jarrin N, Revell A, Prosser R, Laurence D (2009) Reconstruction of turbulent fluctuations for hybrid RANS/LES simulations using a synthetic-eddy-method. Int J Heat Fluid Flows 30:435–442

Kempf A, Klein M, Janicka J (2005) Efficient generation of initial- and inflow-conditions for transient turbulent flows in arbitrary geometries. Flow Turbul Combust 74:67–84

Kim J, Moin P, Moser R (1987) Turbulence statistics in fully developed channel flow at low Reynolds number. J Fluid Mech 177:133–166

Klein M, Sadiki A, Janicka J (2003) A digital filter based generation of inflow data for spatially developing direct numerical or large-eddy simulations. J Comput Phys 186(2):652–665

Kondo K, Murakami S, Mochida A (1997) Generation of velocity fluctuations for inflow boundary condition of LES. J Wind Eng Ind Aerodyn 67–68:51–64

Kraichnan R (1970) Diffusion by a random velocity field. Phys Fluids 13(1):22–31

Lee S, Lele S, Moin P (1992) Simulation of spatially evolving compressible turbulence and the application of Taylor's hypothesis. Phys Fluids A 4:1521–1530

Lund TS (1998) Generation of turbulent inflow data for spatially-developing boundary layer simulations. J Comput Phys 140(2):233–258

Majander P (2006) Assessment of an inflow generation method in a channel flow. Report 149, Helsinki University of Technology, 19 pp
Mansoorzadeh S, Pain CC, de Oliveira C, Goddard A (1998) Finite element simulations of incompressible flow past a heated/cooled sphere. Int J Numer Methods Fluids 28:903–915
Nakayama H, Tamura T, Okuda Y (2005) LES study of fluctuating dispersion of hazardous gas in urban canopy. In: 4th European-African conference on wind engineering (EACWE4), Prague, Czech Republic, 11–15 July, 5 pp
Nozawa K, Tamura T (2002) Large-eddy simulation of the flow around a low-rise building immersed in a rough-wall turbulent boundary layer. J Wind Eng Ind Aerodyn 90:1151–1162
Oliveira TF, Miserda RB, Cunha FR (2007) Dynamical simulation and statistical analysis of velocity fluctuations of a turbulent flow behind a cube. Math Probl Eng 2007:28
Pain CC, Umpleby AP, de Oliveira CRE, Goddard AJH (2001) Tetrahedral mesh optimisation and adaptivity for steady-state for transient finite element calculations. Comput Methods Appl Mech 190:3771–3796
Smagorinsky J (1963) General circulation experiments with the primitive equations. Mon Weather Rev 91: 99–164
Smirnov A, Shi S, Celik I (2001) Random flow generation technique for large-eddy simulations and particle-dynamics modeling. J Fluid Eng 123(2):359–371
Spalart PR, Leonard A (1985) Direct numerical simulation of equilibrium turbulent boundary layers. In: 5th symposium on turbulent shear flows, Ithaca, NY, USA, 7–9 Aug, 5 pp
Taylor GI (1938) The spectrum of turbulence. Proc R Soc Lond A 164:476–490
Thomas TG, Williams JJR (1999) Generating a wind environment for large-eddy simulation of bluff body flows. J Wind Eng Ind Aerodyn 82(1–3):189–208
van Veen L, Kida S, Kawahara G (2006) Periodic motion representing isotropic turbulence. Fluid Dyn Res 38(1):19–46
Wang H (2007) Numerical modelling of pedestrian exposure to traffic pollution at an intersection. PhD thesis, Imperial College, London, 262 pp
Xie ZT, Castro IP (2008) Efficient generation of inflow conditions for large-eddy simulation of street-scale flows. Flow Turbul Combust 81:449–470
Xu S, Martin MP (2004) Assessment of inflow boundary conditions for compressible turbulent boundary layers. Phys Fluids 16(7):2623–2639